Correlation between Current-Voltage Characteristics and DC Field Grading for Dielectric Liquid used in Wet-Mate DC Connector

Mattewos Tefferi[1, 2], Mona Ghassemi[3], Christopher Calebrese[4], Qin Chen[4] and **Yang Cao[1, 2]**
[1]Electrical Insulation Research Center, Institute of Materials Science, [2]Electrical and Computer Engineering University of Connecticut, 97 North Eagleville Road, Storrs, CT 06269-3136, USA, [3] ECE Dept., Virginia Tech, 1185 Perry Street, Blacksburg, VA 24061, USA, [4]GE Global Research Center, Niskayuna, NY 12309, USA

ABSTRACT

Subsea DC transmission and distribution system is a promising technology for powering subsea oil and gas fields with high power, long distance and ultra-deepwater depth. In subsea DC transmission and distribution, wet-mate (WM) connectors are considered as a challenging component due to the complicated electrical field distribution in the insulation system and harsh undersea wet-mating environmental conditions. In order to design reliable liquid insulation systems for subsea connectors, it is essential that the behavior of the DC-stressed liquid insulation be fully characterized for thorough understanding. In this paper, liquid conduction phenomena in synthetic ester oil are studied using the current-voltage characteristics and electric field distribution mapping based on the Kerr electro-optic effect. The correlations between the current-voltage characteristics and DC field grading among different electrode gaps and oil types were analyzed. The experimental results suggest that for applied voltage less than the saturation voltage (V_s), the conduction is dominated by ion dissociation in the bulk oil. Correspondingly, the liquid conduction is ohmic and with formation of heterocharges around the contacts giving symmetrical field distribution. At applied voltage higher than saturation voltage (V_s), this bulk conduction will transit to extrinsic dominated conduction with carriers injected through liquid-electrode interfaces. Under such carrier injection, the corresponding field distribution becomes asymmetrical. In addition to the laboratory experiments, computer simulations with an ion drift-diffusion conduction model taking into account electrode injection were carried out to validate the experimental field distribution at different electrode gaps. The effect of electrode material on the electric field distribution in the oil is investigated and implications for wet-mate connector design principles are presented.

Index Terms — **wet-mate DC connectors, non-polar liquids, electric conduction, Kerr effect, moisture content**

1 INTRODUCTION

THE subsea DC transmission and distribution system installed on the seabed is a promising technology for powering subsea oil and gas (O&G) fields with high power (e.g., >100 MW), from a long distance (e.g., > 100 km) and in ultra-deep-water (UDW) (depths up to 3,000 m). For a modularly stacked subsea DC transmission and distribution system, WM connectors are essential components for system field deployment, faulty component isolation and repairing. However, the design and development of WM DC connectors are challenging due to complicated electrical field distribution in the insulation system as well as the harsh subsea environment. A subsea DC connector is not yet commercially available and the research and development of this component are essential for the subsea O&G extraction and processing industry [1, 2].

For WM DC connectors, oil is an integrated part of the insulation system and provides one of the two barriers in the hybrid insulation structure. The reliability of oil insulation is highly important. In proper WM DC connector design, most of the field stress is distributed in solid insulation. However, under transients due to high voltage fault, the stress in oil and along the oil-solid interface can be very high. Therefore, in order to design reliable liquid insulation systems for WM DC connectors, it is important that the behavior of the DC stressed liquid insulation be fully understood. The Kerr effect based field measurement provides a quantitative measure for safe

Manuscript received on 18 September 2017, in final form 28 May 2018, accepted 29 May 2018. Corresponding author: Y. Cao.

DOI: 10.1109/TDEI.2018.007015

design of WM DC connectors. In addition, current-voltage characteristics add value for the understanding the conduction mechanism.

Previous study in transformer oil has shown that a model based on dissociation of ion pairs within liquid bulk can describe the main features of the steady-state field distribution at a low applied voltage with various gap length [3]. However, in the high field regime the above mechanism is unable to describe the conduction characteristics.

In this paper, we propose a field dependent conduction formalism to describe regimes of conduction associated with dissociation and injection ions, based on the experimental study of current-voltage characteristics and DC field distribution measured using Kerr effect on different electrode gaps and applied voltage. The experimental analysis suggests that injection and the dissociation contribute very differently to the total current density, depending on the regime of conduction. For low field (large electrode gap and low applied voltage), the current due to dissociation can be very important. On the other hand, in the high field regime dissociation current is much smaller than the injected current.

2 CREATION OF CHARGE CARRIERS IN NON-POLAR LIQUIDS

The charge carriers in nonpolar insulating oils are mainly created from two sources, with one being the dissociation of ionic pairs in the bulk and the other being the injection of carriers through electrodes [4]. This section starts by defining conduction due to ionic dissociation in bulk liquid dielectrics and the charge generation mechanism in metal/liquid interface. The following information is used to investigate different regimes of conduction and to analyze the results.

2.1 IONIC DISSOCIATION IN BULK LIQUID

Within the framework of the Thomson model of ionic conduction in dielectric fluids [5], the conduction process is controlled by two mechanisms: dissociation of neutral molecules into ionic species and their recombination back to neutral molecules [6],

$$A^+B^- \underset{k_r}{\overset{k_D}{\rightleftarrows}} A^+ + B^- \tag{1}$$

where A^+ and B^- are the free ions dissociated from the neutral pair A^+B^-, and k_D and k_r are the dissociation and recombination constants, respectively.

Free ions are continuously being generated from the dissociation of ionic pairs and conversely, ionic pairs are formed by recombination of ions. The process of positive and negative charge generation can be written with the following rate equation [7],

$$\frac{\partial p}{\partial t} = \frac{\partial n}{\partial t} = k_D c - k_R p n \tag{2}$$

where p and n are the densities of positive and negative ions and c is the density of the ion pairs.

Using the Langevin approximation, the recombination constant can be found [7],

$$k_R = \frac{q(\mu_+ + \mu_-)}{\epsilon_0 \epsilon_r} \tag{3}$$

where $q = 1.602 \times 10^{-19}\, C$ is the magnitude of electronic charge, μ_+, μ_- are the mobility values of positive and negative ions, $\epsilon_0 = 8.85 \times 10^{-12}\, F/m$ is the permittivity of vacuum and ϵ_r is the oil relative permittivity.

In the presence of electric field, Onsager's field enhanced dissociation rate is found in [6],

$$k_D = K_D^0\, F(E) \tag{4}$$

where K_D^0 is the dissociation constant at thermodynamic equilibrium and $F(E)$ is field enhancement function of the electric field which is given by,

$$F(E) = \frac{I_1(4b)}{2b} \tag{5}$$

where I_1 is the modified Bessel function of the first kind, and b is given by,

$$b = \sqrt{\frac{q^3 E}{16\pi\epsilon_0\epsilon_r k_B^2 T^2}} \tag{6}$$

where E is the electric field strength, k_B is the Boltzmann constant and T is the absolute temperature.

In equilibrium state, from Equation (4) the dissociation rate in the absence of electric field is given by,

$$K_D^0 = k_R \frac{n_0^2}{c} \tag{7}$$

The concentration of the ions at thermodynamic equilibrium is related to the ohmic conductivity of the oil through

$$p_0 = n_0 = \frac{\sigma_0}{q(\mu_+ + \mu_-)} \tag{8}$$

When an external electric field is applied, the charge carriers are separated due to the electrostatic forces and move towards the electrode having opposite sign of the applied potential. They experience drift and diffusion and their drift velocity can be defined by their mobility.

$$W_\pm = \mu_\pm E \tag{9}$$

The applied electric field causes diffusion of ions due to the buildup of ion distribution. The diffusive fluxes of the ions are proportional to the gradient of the ions densities. The diffusion coefficients are defined by Einstein's relation,

$$D_\pm = \frac{k_B T}{q}\mu_\pm \tag{10}$$

Equation (2) can be extended considering ionic drift and diffusion, which describes transport of charges through the bulk of fluid:

$$\begin{cases} \dfrac{\partial p}{\partial t} + \nabla \cdot (\mu_+ E p - D_+ \nabla p) = k_D c - k_R p n \\ \dfrac{\partial n}{\partial t} - \nabla \cdot (\mu_- E n + D_- \nabla n) = k_D c - k_R p n \end{cases} \tag{11}$$

Equations (11) contain field dependent coefficients. Furthermore, relationship between electric potential and charge density is governed by Poisson's equation. This allows for obtaining electric field distributions in the liquid in the presence of space charge.

$$\nabla \cdot (\epsilon_0 \epsilon_r \nabla \varphi) = -q(p - n) \tag{12}$$

2.2 INJECTION AT THE LIQUID METAL INTERFACE

At locally high field near an electrode, ion injection can take place. The injection in non-polar liquids occurs in two steps: ions are created on the electrode and then injected into the liquid by overcoming the image-force barrier [4,8-10].

Suppose we have an ion pair A^+B^- near the anode. In the first step, an electron carried by B^- is transferred into the electrode metal by the following reaction,

$$M + A^+B^- \rightleftarrows M(e) + A^+B \tag{13}$$

where M is the metal electrode. The above reaction leads to the creation of A^+B^- on the surface of the electrode. In the second step, A^+ is separated from the pair and emitted to the bulk, to make a free ion [9].

$$(A^+B^-)_{interface} \rightleftarrows (A^+/B^-)_{free} \tag{14}$$

Skipping the lengthy derivation here, the final equation for the injected charge density q_i is given by [4,7,10],

$$q_i = \frac{Aq_0}{2bK_1(b)} \tag{15}$$

where A is constant that relates the ion density at the emitting electrode to the ion density in the bulk at thermodynamic equilibrium. $A \approx 1$ in most of dielectric liquids [7]. q_0 is charge in the bulk and K_1 is the modified Bessel function of the second kind and order one.

3 CONDUCTION REGIMES

It has already been observed that the current-voltage curves drawn in most polar and nonpolar liquid dielectrics bear strong analogy [11] with the ones obtained in a gas subjected to ionizing radiation [5], for which there are three regions: 1) ohmic behavior at low fields, 2) saturation plateau at medium voltage, and 3) fast increase of the current at higher voltage. However, experimental curves for pure liquids hardly show a true saturation plateau [12-14]. Once the conduction reaches the saturation level, injection takes place immediately.

A useful parameter to distinguish the regions of conduction is the ratio between the transit time and ionic relaxation time [15],

$$C_0 = \frac{t_m}{t_r} = \frac{\sigma_0 d^2}{(\mu_+ + \mu_-)\epsilon_0 \epsilon_r V} \tag{16}$$

where t_m the transit time, t_r is the relaxation time, σ_0 is the low field conductivity, and d is the distance between the electrodes.

3.1 QUASI OHMIC REGIME

At low field, the current appears to be a linear function of the applied voltage and obeys Ohm's law. In this regime, transit time of ions is much longer than the relaxation time of the liquid ($C_o \gg 1$). The total current results mainly from dissociation in the bulk. The current density is given by [15],

$$J_0 = \sigma_0 E \sqrt{F(b)} \tag{17}$$

The field distribution in this regime follows a general parabolic curve, as shown in Figure 1b, due to heterocharges accumulate near the surface of the electrodes. The dissociation of impurity in the bulk of the liquid accounts for the source of charge carriers. The continuous creation of anions or cations from molecules in the whole bulk of liquid (Equation (1) reaction) results in the space charge formation near electrodes, i.e., positive charges near the cathode, and negative ones in the vicinity of anode.

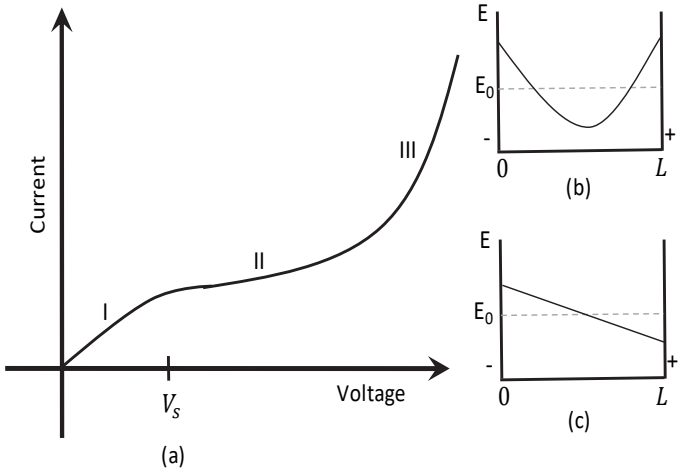

Figure 1. (a) Typical voltage-current characteristics: (b) Distortion of the electric field distribution between parallel plate electrodes with spacing d at voltage V (average electric field is $E_0 = {}^{V}/_{d}$) due to heterocharges; (c) Field distortion due to unipolar positive charge injection.

3.2 SATURATION REGIME

This regime has a smaller transit time than relaxation time and a sweep-out of ions occurs ($C_o \ll 1$). A new equilibrium is then established, where the conduction is limited by the dissociation process. Conduction current is defined by [15],

$$J_s = k_D(E) q c d \tag{18}$$

The transition from ohmic to saturation region occurs when $J_0 = J_s$. The voltage at which the saturation occurs is given by [15,16],

$$V_s = \frac{\sigma_0 d^2 \sqrt{F(b)}}{(\mu_+ + \mu_-)\epsilon_0 \epsilon_r} \tag{19}$$

From the theoretical current-voltage characteristics (Figure 1), the current is expected to be constant starting from the saturation voltage (V_s). However, in dielectric liquids of high resistivity, the saturated current in this regime is often overshadowed by the injection current [7,13-14]. In a real

experiment, a constant current is rarely observed as injection typically starts to take place right after V_s. As a result, most liquids do not exhibit a distinctive saturation plateau because the injected current will be the major contributor of the total conduction current [7,12-14].

3.3 INJECTION REGIME

The rapid increase of current at higher voltage is mainly due to the injection of charge carriers. Assuming positive unipolar injection, i.e., the positive electrode as a source of injected charge carriers and collected at ground electrode. The injected current density can be defined by knowing the density of injected charges [7, 10],

$$J_i = \mu q_i E_{inj} \tag{20}$$

where J_i is the injected current density, q_i is injected charge density (given by Equation (15)) and E_{inj} is the electric field at the surface of the injecting electrode and can be considered as equal to the mean field if the injection is weak.

The total conduction current is the sum of injected current and dissociated current. As it will be shown in the next section, at low field ($V < V_s$), dissociation current will be the major source of conduction current and at high field ($V > V_s$) the total current density has the injected current as a major contributor.

4 EXPERIMENTAL INVESTIGATION

In this work, liquid conduction is studied experimentally by two methods: (a) the voltage-current characteristics, and (b) the electric field distribution measurement by the Kerr electro-optics. The correlation between the current-voltage characteristics and DC field grading among different electrode gaps as well as purity of liquid gives a full insight and understanding of the conduction mechanisms in liquid dielectrics.

4.1 SAMPLE PREPARATION

Synthetic ester oil, a common type of oil for subsea insulation, is used in this study. The dielectric properties of the insulating oil are highly sensitive to moisture and contaminants which affect the DC field distribution. Therefore, to understand the impact of moisture and ionic contaminants on the electric field distribution, three oil samples further indicated as oils A, B and C were prepared. Oil A is a fresh synthetic ester oil degassed and filtered for at least 24h prior to experiment. Oil B was prepared by introducing deionized water (740 ppm) to oil A. Oil C was prepared by introducing instant ocean water (200 ppm) which contains dissolved salt (Na^+, Cl^-) as well as other minor ionic species such as Mg^{++} and SO_4^{--}. The experimental procedure designed to introduce different levels of moisture into oil B and oil C was as follows. Initially, the oil was dried under high vacuum at 100 ^oC for 24 hours for moisture removal. Then deionized water or instant ocean water was added to the dried oil by micropipette. In the next step, the container was sealed and vigorously shaken by a Burrell shaker for 6 hours to form water-in-oil emulsions. Finally, the samples were ultrasonicated for 3 hours until no water was observed at the bottom of the sample holder. As such, the water was considered to be well dissolved into the oil. Measurement of water concentration in oil was performed using Domino Dss from Doble Engineering.

4.2 CURRENT-VOLTAGE CHARACTERISTICS

The investigation of the influence of electrode gap and purity of the oil on the conduction current was carried out by monitoring the quasi steady-state current with a Keithley picoAmp meter for samples subjected to DC bias provided by a Spellman high voltage DC supply. The test cell containing two circular brass electrodes was filled with ~500 mL of oil and kept in dry and clean laboratory conditions.

4.3 KERR ELECTRO-OPTICS SET UP

Kerr electro-optic measurement system was developed to probe the electric field distribution in liquid insulators. One of the advantages of the Kerr electro-optic measurement technique is that the measurement device does not disturb the original electric field distribution. The schematic for the Kerr electro-optic measurement setup is shown in Figure 2. The laser beam from a 10 mW HeNe laser (wavelength 632.8 nm) first passes through a linear polarizer and then a quarter waveplate to be linearly and circularly polarized, respectively. For enhancing the detection sensitivity, an AC low voltage (200 V, 1 kHz) is superimposed on the applied DC voltage for Lock-in amplification. Under transverse spatial modulation, a phase retardation is developed between light polarized parallel to and perpendicular to the applied field as a result of Kerr quadratic electro-optic effect. Under AC superimposed DC excitation, the following relationship can be obtained [17,18]

$$\Delta\theta = \frac{I_{1\omega}}{I_{dc}} = 4\pi B L E_{ac} E_{dc} \tag{21}$$

where $I_{1\omega}$ is the first harmonic of light intensity, I_{dc} is the dc component of light intensity, B is Kerr constant and L is the electrode length. E_{dc} and E_{ac} are the applied DC electric field and superimposed AC electric field, respectively.

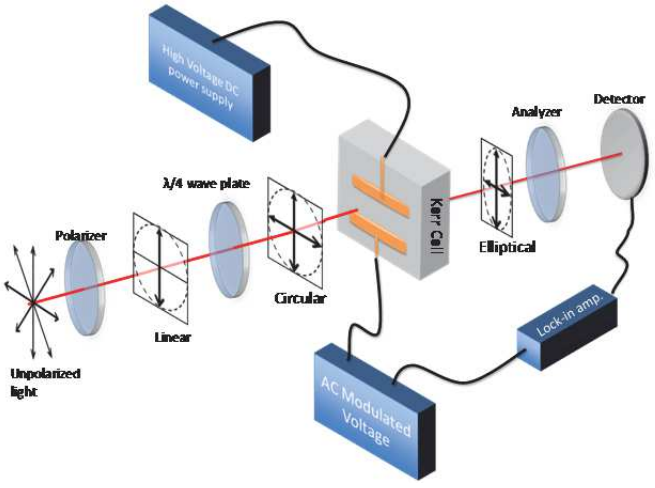

Figure 2. Experimental setup for electric field measurement in insulating oil using Kerr electro-optics effect.

The Kerr test cell is made of high transmission glass sealed on plastic standoffs. A pair of brass parallel-plane electrodes each with an area of 25 cm^2 and thickness of 4.5 mm were used. Measurement of position dependent electric field across the oil gap is achieved by using a linear translation stage. At each measurement point, the light through an analyzer was detected using a photodetector, PDA 10A, the AC output of which was measured with a SR830 DSP lock-in amplifier.

The WM connectors must satisfy the requirements related to deep-sea installation and operation. This means the electrical insulation in the connector needs to be exposed to high-pressure seawater during underwater mating process. With the pressure-compensated design, the insulation system is also subjected to high pressure after mating is completed. However, prior research on the effect of pressure on synthetic ester oil [19] shows the conductivity is highly dependent on water content and applied field and nearly independent of the pressure. High field conduction study also suggests that the current-voltage characteristics show no pressure dependence (0.1-10 MPa) [15]. In the current paper, instead of addressing the dynamical effect of pressure we focus on effects of electrode configuration, gap separation and moisture and contaminants.

5 EXPERIMENTAL RESULT AND ANALYSIS

5.1 CURRENT-VOLTAGE CHARACTERISTICS

The experimental voltage-current characteristics for the three oil samples with electrode spacing of 10 mm are shown in Figure 3. All the three oils have common characteristics. i) At low field, the total current density follows ohmic relation. In this region, the dissociation current accounts as the major contributor to the total current density. The measured current density follows the theoretical current density described in Equation (17)ii) When the voltage increases above V_s, the measured current is no longer linear. The conduction is saturated and the dissociation current does not contribute significantly to the total current. Instead, for ($V > V_s$), the injected current is the major contributor to the total current density. The current density measured in this regime fits well the theoretical injected current density described by Equation (20).

The effect of moisture and contaminant is also clear from the test result present in Figure 3. Under the influence of DC field, the higher the moisture and contaminant, the higher was the current. Higher moisture level in the oil renders in more carrier concentration.

The current measured in Figure 3 is a combination of the injected charge carriers and ions generated by dissociation from ionic pairs. In the bulk of the fluid, the distinction between both currents is not possible because injection charge carriers may recombine with the anions generated by dissociation. However, one can distinguish whether dissociation or injection current is dominant based on the fact that the dissociation current density is proportional to the field enhanced dissociation while the injected current is proportional to the injected charge density at a given field. The nature of the conduction is determined by which component dominates. Since both components are field dependent, the voltage V_s can be considered as a boundary between two conduction regimes.

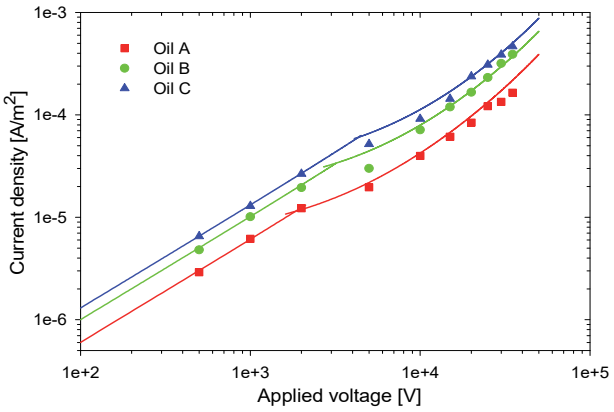

Figure 3. Experimental current-voltage characteristics (log-log) at 10mm electrode gap for oil A, oil B and oil C (symbols). The theoretical current density (solid line) have been computed based on Equations (17) and (20).

From Equation (19), the saturation voltage V_s is dependent on the conductivity and electrode separation. A well-accepted value for ionic mobility in synthetic ester oil is $1 \times 10^{-7}\, m^2/_{Vs}$ [20]. Ohmic conductivities measured at a low field for oil A, oil B and oil C are $6 \times 10^{-11}\, S/_m$, $10 \times 10^{-11}\, S/_m$, $13 \times 10^{-11}\, S/_m$, respectively. The relative permittivity of all oil types is 3.2. Using these values, the saturation voltage as a function of electrode gap is plotted in Figure 4 by solving Equation (19).

Figure 4 shows the variation of V_s as a function of electrode gap for the three oils. For the 10mm electrode gap, V_s is ~1kV for oil A and V_s is ~2 kV for oil B and oil C. When the electrode gap increases to 20mm, V_s increases to 4.5, 7.5 and 10 kV, respectively. Distinguishing the regimes of conduction will help to explain the field measurement in Section 5.2.

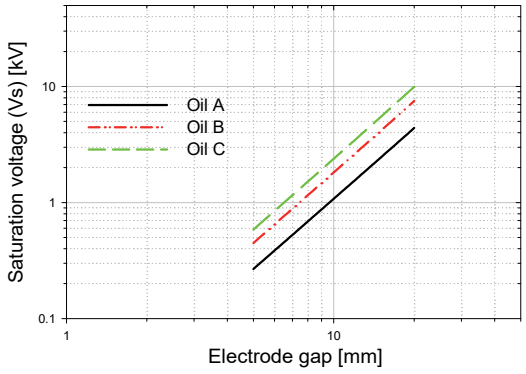

Figure 4. Variation of V_s as a function of electrode gap for oils A, B and C.

Figure 5 shows the conduction current for oil A with various gap settings. V_s depends on the gap separation. For small gap V_s is generally low and it increases with gap separation. It is clear from Figure 5 that the measured current

density follows initially ohmic and then injected current density. Oil B and oil C also show similar behavior.

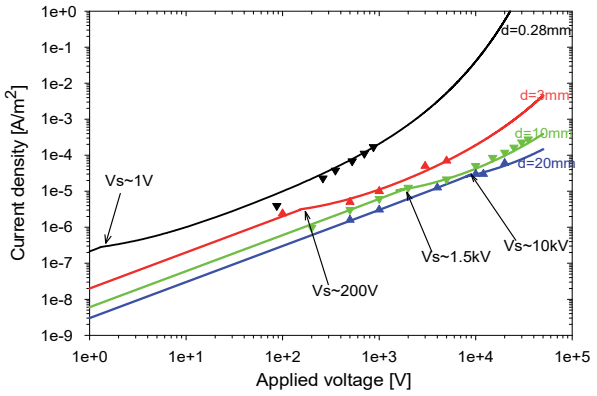

Figure 5. Experimental current-voltage characteristics (log-log) corresponding to oil A with different electrode gaps (symbols). The theoretical current density (solid lines) have been computed based on Equations (17) and (20).

5.2 DISTRIBUTION OF THE FIELD IN THE VARIOUS CONDUCTION REGIMES

Most early Kerr electro-optics field mapping studies were performed on liquids with a very strong Kerr effect, such as nitrobenzene or propylene carbonate [21, 22]. Non-polar liquids such as transformer oil and synthetic ester oil have Kerr constant almost four to five orders of magnitude smaller than that of nitrobenzene or propylene carbonate. Lock-in amplification has to be employed to enhance the Kerr electro-optic measurement sensitivity.

The Kerr constant of the synthetic ester oil used in this study was determined to be $7.56 \times 10^{-16} \frac{m}{V^2}$ by measuring the ratio of $I_{1\omega}/I_{dc}$ as according to Equation (21). The measurements were carried out in synthetic ester oil under low field where the aforementioned ratio is linearly proportional to the applied electric field intensity. Within the range of this study, the Kerr constant of the synthetic ester oil was found to be constant in spite of the presence of deionized water or instant ocean water. The Kerr constant of $7.56 \times 10^{-16} \frac{m}{V^2}$ was used in subsequent field measurement for the characterization the oil across different oil gaps and voltage variations.

The combined effects of electrode gap and oil type on the field distribution are shown in Figures 6, 7 and 9. In Figure 6, the electrode gap was set to 20 mm and three different voltage levels (4, 12 and 20 kV) were applied and field distribution in various regimes can be observed. For 20 mm electrode gap, 4kV lies below V_s. Therefore, dissociation of impurity in bulk oil is the source of charge carriers. Charge dissociation causes heterocharge distributions as a positive charge is attracted to the cathode and negative charge is attracted to the positive electrode. This tends to increase the magnitude of electric field near electrodes which gives a symmetrical U shape of electric field distribution [3]. These results are consistent with the ohmic current-voltage characteristics determined experimentally for large oil gap under low voltage.

When the applied voltage increases to 12 and 20 kV, an asymmetric field distribution is observed. The field linearly decreases from cathode to anode which implies the presence of positive ions in the oil gap. This is due to injection of charge carriers created by exchange at the liquid metal interface. This is in line with the measured voltage-current characteristics that at high field ($V > V_s$) injection is the major contributor of the total conduction current.

For the three oil types, there is obviously a correlation between the field distortion and the oil type. Oil C shows the strongest field enhancement when compared with oils A and B. The increase of conductivity due to moisture and contaminant appears to make the electric field distribution further non-uniform.

From Figure 6 it is clearly seen that field enhancement reduces with the increase of the applied voltage. This can be explained by the ratio between the transit time and the ionic relaxation time (Equation (16)). When t_r>t_m, the charge carriers are effectively swept out of the gap as soon as they are created and before they have time to recombine with a counter ion. This results in only minor space charge. When t_m>t_r, i.e., the relaxation time is faster than the transit time, ions are rapidly recombined with counter ion before it has traveled any significant distance in the oil gap. In the center of the gap, it will have essentially equilibrium condition with positive and negative ions canceling each other. However, near the electrode, a layer of space charge exists.

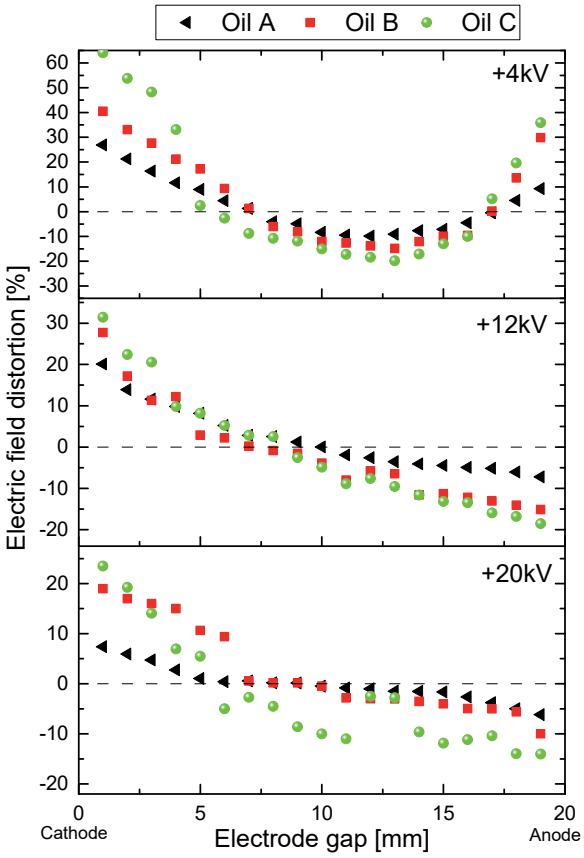

Figure 6. Measured relative field distortion for oil A, B and C over 20mm oil gap at three different applied voltage (4, 12 and 20 kV).

Similar field distribution was observed in [3] as reproduced in Figure 7. At low field (0.1-0.3 kV/mm), the electric field as a function of position in the oil gap follows a parabolic shape. This behavior was explained by an ion drift model without injection. The swept of ion pair dissociation in the oil gives rise to the formation of heterocharges around the contacts. These heterocharges increase the field close to the electrodes and give a field minimum in the middle of the gap. At moderately high field (~1kV/mm), a different type of field distribution is found. The field constantly increases going from the positive electrode to the negative electrode. This type of field distribution was explained in [3] by considering the mobility disparity between positive and negative ions by a factor of four. However, more recent studies [20, 23] show that such polarity dependent disparity in ionic mobilities does not exist. In our present study, the transition from symmetrical to asymmetrical field distribution can be explained by field dependent injection of charges from the electrode(s).

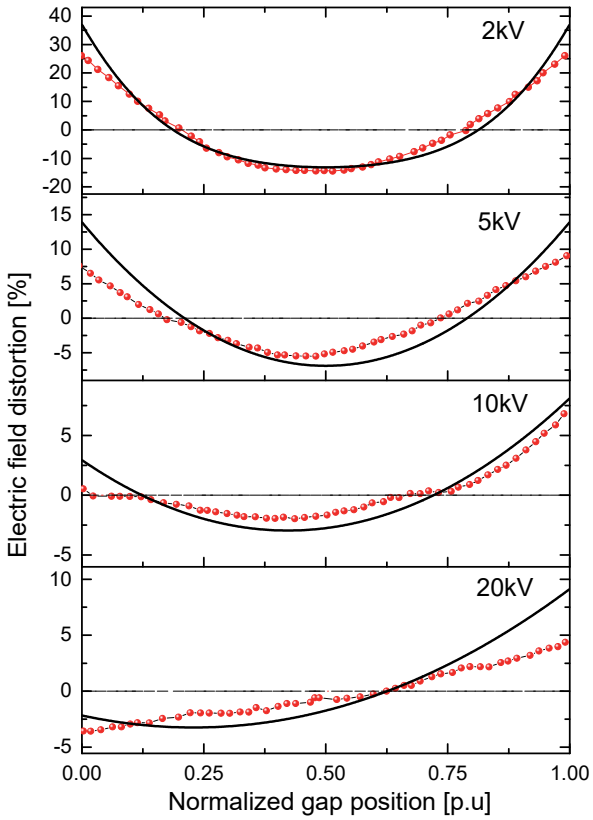

Figure 7. Relative field distribution (distortion) for transformer oil with 19mm electrode gap and applied voltage of 2, 5, 10 and 20 kV with data taken from [3]. Symbols represent the Kerr measurement data from [3]. The solid lines denote the computation based on ion drift model. At 2 and 5 kV, the field distributions are symmetrical U shape. The calculated field distribution from ionic drift model [3] is in agreement for low voltage. At 10 kV, a small deviation from symmetrical to asymmetrical is observed. At 20 kV, it is clear that the field is strongly asymmetrical. This suggests the presence of positive ions. Based on a unipolar injection induced positive ion formation model (instead of ion mobility disparity), field distribution was computed with the boundary condition defined in Equation (15), resulting in a good fit to the measurement data from [3] for under 20 kV. The value of A used in the computation is ~0.25.

The theoretical variation of the current density with applied voltage is calculated based on experimental data retrieved from [3] for transformer oil to further study the transition fromsymmetrical to asymmetrical field distribution. As shown in Figure 8, the current is linear for applied voltage up to 8 kV and it shows tends to saturate. Starting at 10 kV injection current begins to dominate.

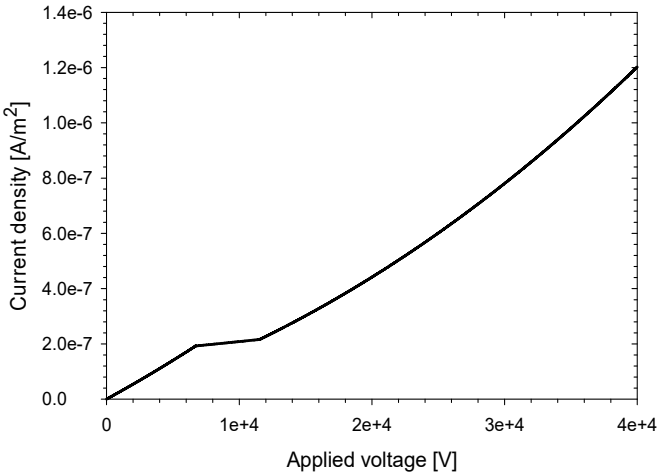

Figure 8. Theoretical current-voltage characteristics calculated using $\sigma_0 = 5 \times 10^{-13} S/m$, $\mu_{\pm} \cong 10^{-9} S/m$, $\epsilon_0 = 2.2$ for the transformer oil in [3].

The general U shape of low voltage curves (up to 10 kV) in Figure 7 shows that hetercharges accumulate near the electrode. This indicates that dissociation of impurities in the bulk of the liquid is the source of the charge carriers. This is in very good consistency with our computed current-voltage characteristics. As shown in Figure 8, the current obeys ohmic conduction for applied voltage up to 8 kV. Once the applied voltage is higher than the saturation voltage level the previously bulk conduction will transit to extrinsically dominated conduction with carriers injected through liquid-electrode interfaces, resulting in an asymmetrical field distribution.

Figure 9 shows the field distribution when the electrode gap is reduced to 10mm. Within all applied voltage ranges shown in Figure 9, it can be seen that the electric field is low near the positive electrode and high near ground electrode. This field distribution implies the injection of positive ions. This is in general agreement with the current-voltage characteristics curve measured at 10 mm electrode gap. From Figure 3, for the voltage applied above 1kV, the measured current follows the injection model developed on unipolar positive injection current.

5.3 COMPUTER SIMULATIONS FOR FIELD DISTRIBUTION IN SIMPLE OIL GAP

The Kerr electro-optic experiment data of electric field distribution were fed into an ionic drift conduction based computational model. The ionic drift model is implemented and solved in Comsol Multiphysics under 1-D configuration for different oil gaps. Governing equations for the ionic drift model are described in Section 2.1.

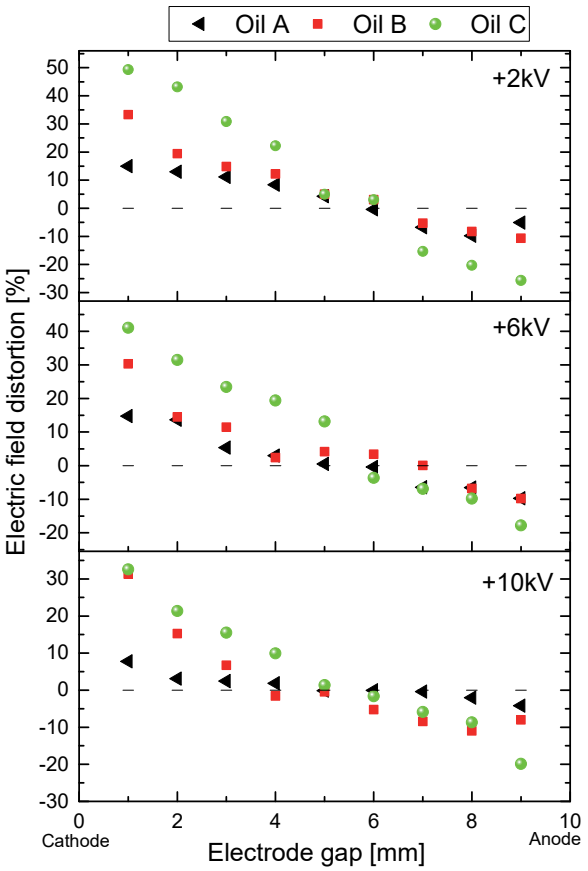

Figure 9. Measured relative field distortion for oils A, B and C over 10mm oil gap at three different applied voltages (2, 6 and 10 kV).

5.3.1. BOUNDARY CONDITIONS

Electrical boundary conditions for Equation (12) on the surfaces of metallic electrodes are known potentials

$$U(0) = 0 \qquad U(d) = U_a \tag{22}$$

For applied voltage less than V_s the simulation is carried out without considering the effect of charge injection from the electrodes. For applied voltage higher than V_s, unipolar positive charge injection was implemented on the surfaces of the positive electrode. The expressions for injected charge density was derived in Equation (15). Assuming a unipolar injection, an injection strength of A≈0.75 gives the best match to the experimental data.

Figures 10 and 11 show the simulated field distributions for corresponding cases shown in Figures 6 and 9, respectively. The overall field distribution from the simulation can be found in general agreement with the measurement results. Under high fields, there are deviations between the experiment and simulation of the magnitudes of electric fields, particularly near the electrodes. This may be caused by the electrohydrodynamic motion (EHD). While care was taken to exclude the EHD, any EHD motion will lead to the overestimation of the space charge effect simply based on time and space averaging performed by the measurement system.

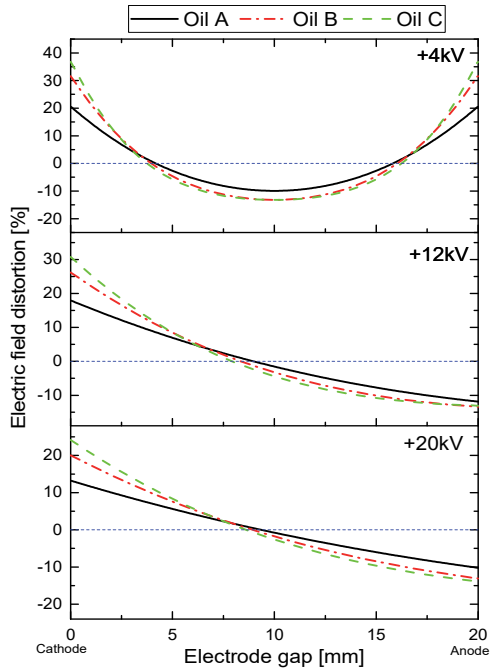

Figure 10. Simulated relative field distortion for oils A, B and C over 20mm oil gap at three different applied voltages (4, 12 and 20 kV).

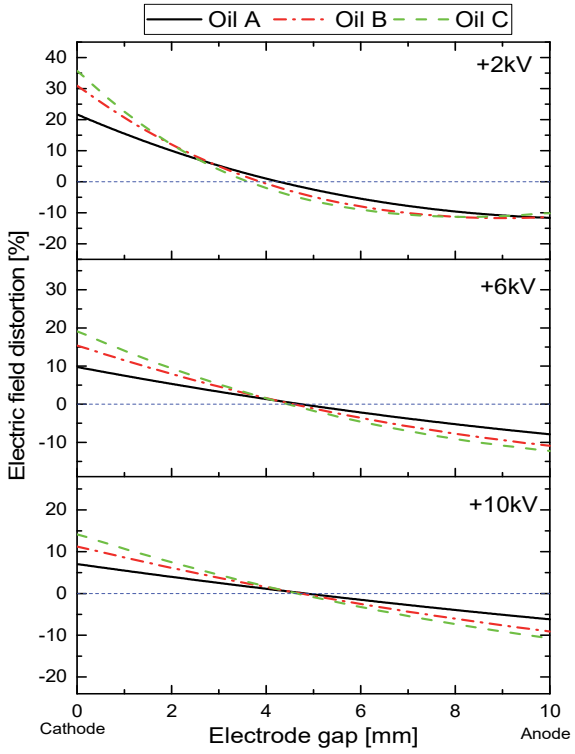

Figure 11. Simulated relative field distortion for oils A, B and C over 10mm oil gap at three different applied voltages of 2, 6 and 10 kV, respectively.

6 EFFECT OF ELECTRODE

Charge injection will lead to the distortion of the electric field distribution in oil gap. Therefore, the effects of electrode material on the charge inject and field distortion shall be investigated. Three types of electrode materials

(brass, stainless steel, and aluminum) were employed in this study.

Figure 12 shows the electric field distribution of oil A at 10 mm electrode gap under 10kV with different electrode materials. As shown in the figure, the field profile across the oil gap with each electrode material differs and the magnitude of field distortion appears to be with good correlation with the work function. As shown in Table 1, due to a high work function of stainless steel compared with brass and aluminum, the quantity of space charge injected is significantly less than the aluminum and brass electrode under the same applied voltage. Not only this study suggests charge injection under high field a plausible mechanism but also forms a basis for design optimization through proper electrode design.

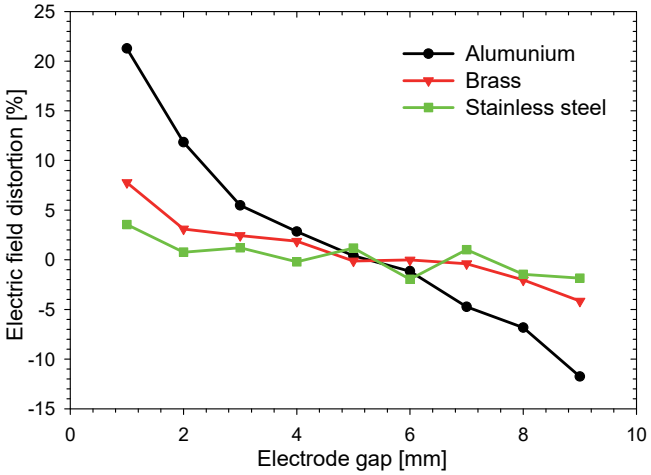

Figure 12. The influence of electrode material on the electric field distribution. The relative electric field distortion for an aluminum electrode is significantly higher than for brass and stainless steel.

Table 1. Electrode work function [24].

Electrode material	Work function [eV]
Stainless steel	5.05
Brass	4.50
Aluminum	4.20

7 IMPLICATIONS FOR WET-MATE CONNECTORS DESIGN

There is a desire to design WM connectors to be reliable and more compact. This is due to the increasing demand for higher voltages and power ratings. In order to have an optimal design of WM connectors, the DC grading that the oil is subjected has to be well understood. One important factor in the design of WM connectors is to determine the maximum acceptable field level so that the field distribution does not exceed these levels to ensure reliable operation. Currently, there are no industrial standard or design rules available that specify the design field level for DC connectors. Therefore, one way to estimate an acceptable field level can be based on the field distortion level. In the absence of space charge, the field applied is nearly equal to the average applied field (Laplacian field). In case of space charge accumulation, the average electric field will be distorted.

As described in Section 5.2, the electric field distribution has a different degree of distortion depending on the electrode gap. The electric field distribution was computed using ionic drift-diffusion model presented in Section 5.3 for electrode gap ranging from 5 to 20 mm and field ranging from 0.2 to 1kV/mm. The percentage of field distortion is shown in a contour plot (Figure 13).

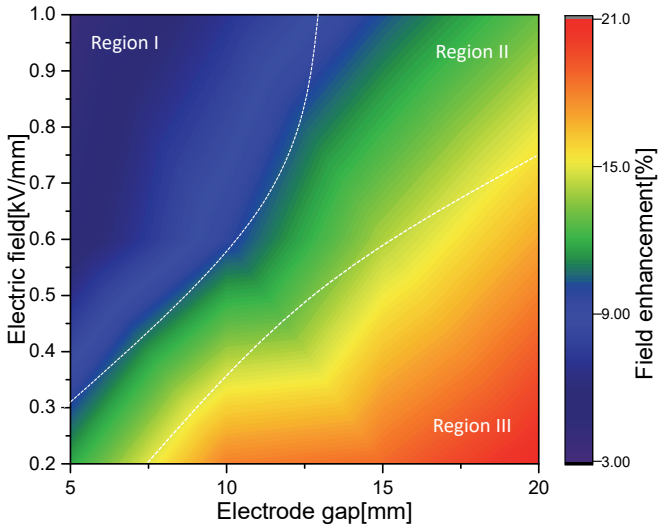

Figure 13. Electric field enhancement at different applied fields for various electrode gaps.

Three regions are clearly seen from Figure 13. Region 1 possesses small field enhancement with a narrow gap. Region 2 corresponds to medium field enhancement at a medium gap. Region 3 marks high field distortion with wider gaps. Region 3 is unfavorable as high field distortion leads to early be failed. Such contour plot shall provide a quantitative basis for the design trade-off study for oil gap.

8 CONCLUSIONS

In this paper, the experimental investigation results of a liquid insulation system envisioned for DC WM connector were presented. A Kerr electro-optic technique was developed to characterize the insulation performance of the liquid insulation system with different electrode gaps and applied voltages. The electric field distribution in different conduction regimes has been examined, and it was shown that the current-voltage characteristics could well justify the transition from symmetrical to asymmetrical field distribution. At low voltage, conduction is mainly due to dissociation of ions from bulk liquid and at high field conduction is mainly the consequence of injection from the interface. Moreover, effects of moisture and ionic contaminants as well as effect of electrode material on the electric field distribution in the oil were investigated.

The presented ionic drift-diffusion model has shown the ability to predict the behavior of the electrical fields at

different regimes which agrees well with the Kerr measurements. From the field measurement result, electric field distortion can be designed to be very low provided that the separation between the solid barriers in the hybrid insulation structure be narrow. This study of oil DC characteristics will be a valuable input to promote in-depth understanding of solid-liquid insulation systems implemented in WM connectors [25,26].

ACKNOWLEDGMENT

Funding for this work is provided by RPSEA through the "Ultra-Deepwater and Unconventional Natural Gas and Other Petroleum Resources" program authorized by the U.S. Energy Policy Act of 2005. RPSEA (www.rpsea.org) is a nonprofit corporation whose mission is to provide a stewardship role in ensuring the focused research, development, and deployment of safe and environmentally responsible technology that can effectively deliver hydrocarbons from domestic resources to the citizens of the United States. RPSEA, operating as a consortium of premier U.S. energy research universities, industry, and independent research organizations, manages the program under a contract with the U.S. Department of Energy's National Energy Technology Laboratory.

REFERENCES

[1] GE Global Research Report, MSDC Electrical System for Deepwater Subsea Process, Contract No. 08121-2901-01, Nov. 2013

[2] GE Global Research Report, Subsea High Voltage Direct Current Connectors for Environmentally Safe and Reliable Powering of UDW Subsea Processing, Contract No.12121-6302-01, April 2015.

[3] U. Gafvert, A. Jaksts, C. Tornkvist, L. Walfridsson, "Electrical field distribution in transformer oil", IEEE Trans. Electr. Insul., vol. 27, pp. 647-660, 1992.

[4] A. Alj, A. Denat, J.P. Gosse, B. Gosse, "Creation of charge carriers in nonpolar liquids", IEEE Trans. Electr. Insul., vol.20, pp. 221-231, 1985.

[5] J.J. Thomson and G.P. Thomson, *Conduction of Electricity through Gases,* Cambridge University Press, London, 1928.

[6] L. Onsager, "Deviations from Ohm's law in weak electrolytes", J. Chem. Phys., vol. 2, pp. 599-615, 1934.

[7] F. Pontiga, A. Castellanos, "Electrical conduction of electrolyte solutions in nonpolar liquids", IEEE Trans. Indus. Appl., vol.32, pp.816-824, 1996.

[8] M. Nemamcha, J.P. Gosse, B. Gosse and A. Denat "Influence of Insulating Electrode Coating on the Electrical Conduction of Cyclohexane", IEEE Trans. Electr. Insul., vol.23, pp. 529-534, 1988.

[9] Yong Kweon Suh, "Modeling and simulation of ion transport in dielectric liquids - Fundamentals and review", IEEE Trans. Dielectr. Electr. Insul., vol.19, pp.831-848, 2012.

[10] A. Denat, B. Gosse and J.P. Gosse, "Ion Injections in Hydrocarbons", J. Electrostat., vol.7, pp. 205-225, 1979.

[11] W. F. Schmidt, "Elementary processes in the development of the electrical breakdown of liquids", IEEE Trans. Electr. Insul., vol.17, pp. 478-483, 1983

[12] A. Nikuradse, *Das flüssige Dielektrikum* (Springer, Berlin), 1934.

[13] N. J. Felici, "A tentative explanation of the voltage-current characteristics of dielectric liquids", J. Electrostat., vol. 12, pp. 165–172, 1982.

[14] J.C. Fillipini, "Recent Progress in Kerr Cell Technology, Physical Considerations", J. Phys. D. Appl. Phys., vol. 8, pp. 201–213, 1975.

[15] A. Denat, "Conduction and breakdown initiation in dielectric liquids", *IEEE Int. Conf. Dielectric Liquids (ICDL*), 2011, pp. 1-11.

[16] A. Denat, B. Gosse, J.P. Gosse, "Electrical conduction of solutions of an ionic surfactant in hydrocarbons", J. Electrostat., vol. 12, pp. 197-205, 1982.

[17] K. Nakamura, K. Kato, H. Koide, Y. Hatta, H. Okubo, "Fundamental property of electric field in rapeseed ester oil based on Kerr electro-optic measurement", IEEE Trans. Dielectr. Electr. Insul., vol. 13, pp. 601-607, 2006.

[18] T. Maeno, Y. Nonaka, T. Takada, "Determination of electric field distribution in oil using the Kerr-effect technique after application of DC voltage", IEEE Trans. Electr. Insul., vol. 25, pp. 475- 480, 1990.

[19] Torstein G. Aakre, Torbjorn A. Ve, Oystein L. Hestad, "Conductivity and Permittivity of MIDEL 7131: Effect Temperature Moisture Content Hydrostatic Pressure and Electric field", IEEE Trans. Dielectr. Electr. Insul., vol. 23, pp. 2957-2964, 2016.

[20] Y. Jing, I. V. Timoshkin, M. P. Wilson, M. J. Given, S. J. MacGregor, and T. Wang, "Dielectric properties of natural Ester, synthetic ester midel 7131 and mineral oil Diala D", IEEE Trans. Dielectr. Electr. Insul., vol. 21, pp. 644 - 652, 2014.

[21] E. C. Cassidy, R. E. Hebner, M. Zahn, R. J. Sojka, "Kerr-effect studies of an insulating liquid under varied high-voltage conditions", IEEE Trans. Electr. Insul., vol. 9, pp. 43-56, 1974.

[22] A. Helgesonl, M. Zahn, "Kerr electro-optic measurements of space charge effects in HV pulsed propylene carbonate", IEEE Trans. Dielectr. Electr. Insul., vol. 9, pp. 838-844, 2002.

[23] L. J. Yang, S. M. Gubanski, Y. V. Serdyuk, and J. Schiessling, "Dielectric properties of transformer oils for HVDC applications", IEEE Trans. Dielectr. Electr. Insul., vol. 19, pp. 1926 - 1933, 2012.

[24] Qing Yang, Yang Jin, Wenxia Sima, Mengna Liu, "Effect of the electrode material on the breakdown voltage and space charge distribution of propylene carbonate under impulse voltage", AIP Advances, vol.6, pp. 045215 1-8, 2016.

[25] M.Tefferi, M. Ghassemi, C. Calebrese, Q. Chen and Y. Cao, "Characterization of Solid-Liquid Interface for Wet-Mate Subsea HVDC Connectors", *Annu. Rep. Conf. Electr. Insul. Dielectr. Phenom.,* 2016, pp.735-738.

[26] M. Tefferi, M. Ghassemi, C. Calebrese, Q. Chen and Y. Cao "Characterization of Solid-Liquid Interface in a Wet-Mate Subsea HVDC Connector", *Int. Symp. HVDC Cable system*s, 2017.

Mattewos Tefferi received his MSc in electric power engineering from Chalmers University of Technology, Sweden in 2013. He is currently pursuing his Ph.D. degree in electrical engineering at the University of Connecticut.

Mona Ghassemi (S'07-M'13-SM'16) received her M.S. and Ph.D. degrees both with the first honor in electrical engineering from the University of Tehran, Iran in 2007 and 2012, respectively. She spent two years researching as Postdoctoral Fellow at high voltage laboratory of NSERC/Hydro-Quebec/UQAC Industrial Chair on Atmospheric Icing of Power Network Equipment (CIGELE) and Canada Research Chair on Power Network Atmospheric Icing Engineering (INGIVRE), University of Quebec at Chicoutimi (UQAC), QC, Canada from 2013 to 2015. She also was a Postdoctoral Fellow at the Electrical Insulation Research Center (EIRC) of Institute of Materials Science (IMS) at the University of Connecticut from 2015-2017. In 2017, Dr. Ghassemi joined the Bradley Department of Electrical and Computer Engineering at Virginia Polytechnic Institute and State University as an assistant professor. Dr. Ghassemi is a registered Professional Engineer in the Province of Ontario, Canada, Associate Editor of High Voltage (IET) and Associate Editor of International Journal of Electrical Engineering Education. Her research interests include dielectrics and electrical insulation materials and systems, high voltage technology, multiphysics modeling, plasma science, electromagnetic transients in power systems and power system analysis and modeling.

Christopher Calebrese received his B.S. and Ph.D. degrees from Rensselaer Polytechnic Institute in Materials Engineering. He is currently a materials scientist at the GE Global Research Center, Niskayuna, NY, USA, and was previously a Postdoctoral Research Associate at Rensselaer Polytechnic Institute working on dielectric polymer nanocomposites.

Qin Chen is a Senior Electrical Engineer at GE Global Research, where he has been working since 2008. His background is in dielectric materials and electrical insulation systems. His recent work focuses on the development of high voltage direct current (HVDC) components, such as subsea DC connectors, extruded HVDC cables, and HVDC converter transformers. His interest also includes the development of new polymeric and nanocomposite

DC insulation materials, as well as the fundamental study of polarization and electrical charge transport in dielectric materials using both experimental and multi-physics modeling techniques. Besides HVDC systems, his other experiences include the development of high energy density dielectric materials for energy storage film capacitors, design of AC transformers, monitoring and diagnostics of power instruments, and the study of ferroelectric polymers and developing electro-optical devices based on these materials. Qin received his BS degree from Tsinghua University (Beijing, China) in 2003, and his MS and PhD degrees from Penn State University in 2006 and 2008, all in Electrical Engineering.

Yang Cao was graduated with BS and MS in physics from Tongji University in Shanghai, China, and received his PhD from the University of Connecticut in 2002, after which he served as a senior electrical engineer at GE Global Research Center. Since 2013, he has been an associate professor at the Electrical and Computer Engineering Department of the University of Connecticut. His research interests are in the physics of materials under extreme electric field and the development of new dielectric materials, particularly the polymeric nanostructured materials, for energy efficient power conversion and renewables integrations, as well as for novel medical diagnostic imaging devices. He can be reached at yang.cao@uconn.edu